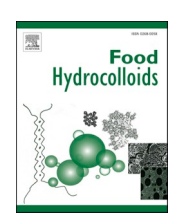
ELSEVIER

Contents lists available at ScienceDirect

Food Hydrocolloids

journal homepage: www.elsevier.com/locate/foodhyd





Super-resolution microscopy reveals heterogeneity in the coverage of oil-in-water food emulsions

Abbas Jabermoradi ^a, Sanam Foroutanparsa ^b, Ilja K. Voets ^b, Jo J.M. Janssen ^c, John P.M. van Duynhoven ^{a,c,*}, Johannes Hohlbein ^{a,d,**}

- ^a Laboratory of Biophysics, Wageningen University and Research, Stippeneng 4, 6708, WE Wageningen, the Netherlands
- b Laboratory of Self-Organizing Soft Matter, Department of Chemical Engineering and Chemistry & Institute for Complex Molecular Systems, Eindhoven University of Technology, P.O. Box 513, 5600, MB Eindhoven, the Netherlands
- ^c Unilever Global Foods Innovation Centre, Wageningen, the Netherlands
- ^d Microspectroscopy Research Facility, Wageningen University and Research, Stippeneng 4, 6708, WE Wageningen, the Netherlands

ARTICLE INFO

Keywords: Super-resolution microscopy Food emulsions Interfacial heterogeneity Phosvitin

ABSTRACT

Oil-in-water food emulsions such as mayonnaise and dressings are stabilized by proteins and low-molecular weight surfactants binding to the oil/water interface. One common source of emulsifying proteins is egg yolk containing the iron-binding protein phosvitin. Here, we applied super-resolution microscopy to quantify the distribution of phosvitin on the droplet interfaces of binary SDS/phosvitin model emulsions prepared by high-pressure homogenization (HPH). We targeted phosvitin either via fluorescently labeled, primary antibodies or with affimers, which are short polypeptides. Re-scan confocal microscopy (RCM) revealed a bimodal droplet size distribution in which small droplets were primarily covered by SDS and large droplets by phosvitin. This interdroplet heterogeneity was in line with expected kinetics of emulsifier coverage of droplet interfaces during HPH. Stochastic optical reconstruction microscopy (STORM) indicated that changing the concentration of phosvitin did not affect the intra-droplet distribution at the droplet interface. STORM further provided a direct visualization of the redistribution of phosvitin upon prolonged low shear treatment, resulting in diffusion-assisted exchange of SDS and phosvitin between droplet interfaces and the continuous aqueous phase. Our RCM- and STORM-based approaches allow a direct and quantitative view on the intricate balance between kinetic and thermodynamic forces governing inter- and intra-droplet interfacial distributions of proteins.

1. Introduction

Food emulsions are intricately structured systems comprising two immiscible liquid phases, usually oil and water, that are stabilized by emulsifiers and mixtures thereof (McClements & Jafari, 2018). Many of these mixtures contain both proteins and low molecular weight (LMW) surfactants. The adsorption of emulsifying proteins at an oil/water interface is influenced by the protein's inherent physical and chemical properties, such as size, charge, conformation, and amino acid composition, as well as environmental conditions like the type of interface (e. g., oil-water, air-water), pH, temperature, and presence of other substances (Rodríguez Patino & Pilosof, 2011). When these proteins adsorb, they stabilize the emulsion through self-interaction, resulting in a viscoelastic layer that resists local deformation (van Aken, 2003). On the

other hand, LMW surfactants are small molecules, each having a hydrophilic head group and one or more hydrophobic tails. Their high mobility allows them to quickly coat the newly formed oil-water interface following the emulsification process (Pugnaloni et al., 2004). Unlike proteins, LMW surfactants form a fluid layer due to the absence of strong intermolecular bonds (Wilde et al., 2004). Moreover, LMW surfactants diffuse laterally towards areas of high surface tension, known as the Marangoni effect (Ewers & Sutherland, 1952). Although the viscoelastic mechanism associated with protein adsorption and the Marangoni mechanism linked to LMW surfactant adsorption both serve to stabilize emulsions, they might not always complement each other and can be mutually unfavorable (Cornec et al., 1998). Formulating protein/LMW emulsifier mixtures has been identified as a route for designing food emulsions with desired physical (McClements, 2015) and

^{*} Corresponding author. Laboratory of Biophysics, Wageningen University and Research, Stippeneng 4, 6708, WE Wageningen, the Netherlands.

^{**} Corresponding author. Laboratory of Biophysics, Wageningen University and Research, Stippeneng 4, 6708, WE Wageningen, the Netherlands. E-mail addresses: john.vanduynhoven@wur.nl (J.P.M. van Duynhoven), johannes.hohlbein@wur.nl (J. Hohlbein).

chemical (Berton-Carabin & Villeneuve, 2023) stability.

Interfacial composition has been identified as a key determinant of the properties of food emulsions (Ravera et al., 2021) and is typically determined by indirect methods (Hinderink et al., 2022, 2024; Niu et al., 2023). Interfacial rheology, for example, can be applied on model films or hanging droplets (Maldonado-Valderrama & Patino, 2010), but does not allow to study the effects of food emulsification routes (Javadi et al., 2022). In food emulsions, the assessment of surface load via the (centrifuged) serum or cream phases is a common and straightforward method to assess interfacial composition. This method is, however, invasive and destructive, and cannot be generally applied to all types of food emulsions (Hinderink et al., 2022, 2024). Spectroscopic methods can be applied to assess conformational changes of proteins at droplet interfaces and their displacement by LMW surfactants, but do usually not provide spatial information (Rampon et al., 2003). Fluorescence microscopy has been identified as a method to assess surface morphology, but so far, this method lacked the capability of resolving protein composition at droplet interfaces (Hinderink et al., 2022). In this work, we will outline an approach based on fluorescence imaging to visualize and quantify surfactant composition at the single-droplet level. We will use a model system for mayonnaise to demonstrate our approach.

To localize proteins and surfactants, the correct choice of fluorescent probes for imaging is critical. In the life sciences, primary or secondary antibodies labeled with fluorescent markers are being widely deployed due to their inherent capability to localize specific biomacromolecules and bind to various targets (Voskuil, 2014). There are challenges with their use, however, including long and unpredictable production timelines, inconsistencies across different production batches that can undermine their effectiveness (Bradbury & Plückthun, 2015), and their large size (approximately 150 kDa) that may limit their ability to penetrate densely packed structures like tissues (Banta et al., 2013; Orlova et al., 2006). A viable alternative to antibodies are affimers, which are small protein scaffolds of about 100 amino acids (Tiede et al., 2014, 2017). Affimers possess a well-defined structure featuring one or two target-specific loops, which enables higher localization accuracy by positioning the probe closer to the target (Schlichthaerle et al., 2018). Affimers are selected through a process known as phage biopanning, which is relatively rapid and effectively minimizes variations between production batches (Banta et al., 2013). As such, affimers can be produced via bacterial expression systems thereby circumventing the expensive and time-consuming traditional routes to obtain antibodies. Together, these features have expanded the use of affimers as specific ligands in bioassays (Tans et al., 2020; Tiede et al., 2017). Their use as ligands that specifically bind to biomolecular targets has also been exploited within the bioimaging field (Hasenhuettl & Hartel, 2019; Schlichthaerle et al., 2018; Tiede et al., 2017), yet their application in food emulsion studies is unexplored.

Mayonnaise is a food emulsion that relies on egg yolk as an emulsifier mixture to maintain its physical and chemical stability (Hasenhuettl & Hartel, 2019). Egg yolk is composed of several constituents, including low-density lipoproteins (LDL), high-density lipoproteins (HDL), phosvitin, and livetin. Upon emulsification, the lipoprotein particles disintegrate, liberating apoproteins and phospholipids as emulsifiers (Anton, 2013). Phosvitin is a highly phosphorylated protein with unique emulsifying, metal-chelating, and pro-oxidant properties among the proteins found in egg yolk (Marcet et al., 2022). In this work we will focus on studying the interaction of phosvitin and SDS, as a model LMW surfactant, at the oil-water interface in emulsions (Jabermoradi et al., 2022). Here, we build on our previous work in which we used super-resolution microscopy techniques to localize proteins in model emulsions for mayonnaise (Jabermoradi et al., 2022, 2024). In particular, we use stochastic optical reconstruction microscopy (STORM) (Rust et al., 2006) to surpass the diffraction limit of traditional fluorescence microscopy and localize phosvitin with molecular specificity at droplet interfaces in binary O/W model emulsions prepared with SDS.

Specifically, we explore fluorescently labeled antibodies and affimers against phosvitin together with buffer conditions that pronounce the blinking of fluorophores. As such, only a subset of fluorophores is fluorescent at any given time, allowing sub 100 nm localization precision of individual emitters rather than looking at overlapping emission (Hohlbein, 2021).

Additionally, re-scan confocal microscopy (RCM) is employed providing higher resolution than conventional confocal microscopy thereby enabling us to resolve smaller droplets. In RCM, the diffraction limited laser excitation spot moving across the field of view is synchronized with a second scanning mirror that reflects the collected fluorescence under twice the original scanning angle onto a camera to obtain an improvement of a factor of sqrt(2) in spatial resolution with minimal technical effort (De Luca et al., 2013). We will first benchmark different strategies to localize phosvitin at droplet interfaces. We will compare the performance of affimer- and antibody-based labelling strategies, and benchmark these against an approach in which phosvitin was labeled covalently with a fluorophore. Next, we will prepare binary emulsions with different phosvitin/SDS ratios with a high-pressure homogenizer (HPH). HPH is a common emulsification method in food processing, known to have an effect on the composition of the droplet surface (Taisne et al., 1996). Further, we investigate the effect of the formulated phosvitin/SDS ratio on the heterogeneity of phosvitin surface coverage and at the intra- and inter-droplet level. Finally, we will investigate the effect of prolonged low shear rate treatment (Kokini & Aken, 2006; Serial et al., 2022) on the interfacial surface coverage with phosvitin.

2. Material and methods

2.1. Isolation and purification of phosvitin

Phosvitin was isolated from fresh egg yolk according to the protocol described by Zhang et al. (Zhang et al., 2011). Fresh hen eggs were obtained from the local market. Egg yolks were separated and rolled on filter paper to remove the chalazas. An equal amount of distilled water was added to the yolk at 4 $^{\circ}$ C, and the obtained solution was centrifuged at 12000 g for 15 min (Avanti j-25, Beckman). The precipitate was collected and homogenized with an equal mass of a 0:17 M NaCl solution, followed by another centrifugation at 12000 g for 15 min. The granules were dissolved in 10 % (w/v) of a 1.74 M NaCl solution. Further, the solution was homogenized with 4 % w/w of PEG6000 and centrifuged at 12000 g for 15 min. The supernatant was dialyzed against distilled water for 24 h at 4 $^{\circ}$ C and subsequently centrifuged at 12000 g for 15 min. The supernatant was collected and lyophilized using a freeze-dryer from either Christ (Germany) or Labconco (United States of America).

2.2. Preparation of binary emulsions

To prepare the binary emulsions, we dissolved lyophilized phosvitin in 0.05 M acetate buffer at pH 3.8 to obtain concentrations of 3, 6, 9 and 12 mg/mL. Each solution was centrifuged at 4000 g for 20 min, and the supernatants were transferred to new aliquots to remove any impurities. We then added 0.15 % w/v of sodium dodecyl sulfate (SDS) to each solution to stabilize the emulsion and investigate the competition between SDS and phosvitin. Next, we added rapeseed oil, 15 % of the final volume, into each of these solutions to prepare the model emulsions. The mixtures were coarsely homogenized using an 18 mm diameter head disperser at 18000 rpm for 2 min, followed by further homogenization at 70 bar using a high-pressure homogenizer (HPH) (Niro Soavi – PandaPLUS 2000; GEA) for ten cycles.

2.3. Low shear treatment

To investigate the impact of low shear treatment on the competition

between phosvitin and SDS, we gently stirred 20 mL of the emulsion prepared with the phosvitin concentration of 6 mg/mL using a magnetic stirrer at a speed of 500 rpm for 3 days.

2.4. Confocal and single-molecule localization microscopy

CLSM imaging was performed using a confocal mode of STED microscope (Abberior Instrument) equipped with UPlanSApo 100x/1,40 Oil [infinity]/0,17/FN26,5 objective (Olympus), a Katana-08 HP laser (Onefive) and multiple laser lines at 405 nm, 488 nm, 561 nm, 640 nm, and the pulsed laser at 595 nm and 775 nm (power = 3 W); plus Imspector 0.14.13919 software. In general, images were acquired with a pixel size of 60 nm and a pixel dwell time of $10~\mu s$. Images were acquired $\approx 2~\mu m$ above the coverslip. A pinhole was set to 1.00~AU at 100x.

For the confocal RCM measurements, we used a Nikon A1R HD25 upright confocal microscope body equipped with an RCM module (Confocal.nl, Amsterdam, Netherlands) (De Luca et al., 2013). The microscope was equipped with a CCD camera (Tucsen, FL 20BW) and four laser lines (405 nm, 488 nm, 561 nm, and 640 nm, Oxxius, France). Images were captured using a Nikon 60x Plan Apo objective lens with a numerical aperture of 1.4. All images were captured in 16-bit format with a resolution of 1024 x 1024 pixels. Micromanager 1.4 (Stuurman et al., 2007), an open-source software for microscope control and image acquisition, was used to acquire RCM images at room temperature. We used the following settings for acquisition: 2.8 mW of 488 nm laser for the oil droplets channel, and 4.6 mW of 647 nm laser for the phosvitin channel, with a frame acquisition time of 4 s.

For STORM data acquisition, we employed a home-built microscope as previously reported (Jabermoradi et al., 2022). A fiber-coupled laser engine (Omicron, Germany) delivered the laser beam to the microscope's excitation path. The beam was collimated using a 60 mm achromatic lens (AC254-060-A-ML, Thorlabs), then deflected by a kinematic mirror (BBE1-E02, Thorlabs) into a top hat beam shaper (Asphericon GmbH). The beam was next focused by a 150 mm lens (AC508-150-A-ML, Thorlabs) into the back focal plane of a 100x oil immersion objective (NA = 1.45, Nikon) via a polychroic mirror (ZT405/488/561/640rpcv2, Chroma). The emitted signal from the sample was collected through the same objective and passed through an emission filter (ZET405/488/561/640m-TRF, Chroma). After being reflected by a kinematic mirror, the signal was focused through a tube lens (MXA20696, Nikon) and into the first lens (AC508-100-A-ML, Thorlabs) of a 4f system. The light was then directed by another mirror to a deformable mirror (DMP40/M - P01, Thorlabs) located in the Fourier plane of the 4f imaging system. Finally, the emitted light was focused via a second lens (AC508-100-A-ML, Thorlabs) onto an sCMOS camera (Prime 95B, Photometrics), with an effective pixel size of 112 nm per pixel. We recorded a total of 10,000 frames per field of view at a rate of 40 ms per frame (25 Hz).

2.5. Conjugation of phosvitin with fluorescein isothiocyanate (FITC) and emulsion preparation

To enable direct fluorescence imaging of phosvitin, we employed a FITC labeling strategy that targeted the primary amines of phosvitin. First, we prepared a solution of phosvitin at a concentration of 6 mg/mL in 0.05 M MES buffer at pH 6.6. Then, we added a freshly prepared solution of 5 mg/mL FITC in DMSO to achieve a final concentration of 0.5 mM. The reaction mixture was stirred for 2 h and subsequently dialyzed for four days using an 8 kDa cutoff dialysis bag (Sigma-Aldrich, Cat. No. D9527). To ensure the complete removal of free dyes, the dialyzed solution was filtered and concentrated using an Amicon® Ultra-15 centrifugal filter with a 3 kDa cutoff (Millipore, Cat. No. C7715). The degree of labeling was then determined by measuring the absorbance of the protein and FITC using a Nanodrop spectrophotometer. The degree of labeling was calculated to be approximately 10 %, assuming that phosvitin has a molecular weight of 35 kD and absorbance

(A280 nm) at 0.1 % (1 g/L) of 0.32 ± 0.02 (L/g.cm) (Castellani et al., 2003). Using this covalently labeled phosvitin solution, we immediately prepared an oil-in-water emulsion by dissolving 0.15 % w/v SDS and adding 15 % (v/v) rapeseed oil. We then proceeded by making a coarse emulsion using an 18 mm diameter dispersing head at 7000 rpm for 2 min (T 18 digital ULTRA-TURRAX, IKA, Germany). We subsequently homogenized the coarse emulsion at 70 bar using a high-pressure homogenizer (HPH) (Delta Instruments LAB Homogenizer) for 20 min and stored the resulting emulsions at 4 °C overnight for further use.

2.6. Phase display selection of phosvitin-specific affimers

Phosvitin-binding affimers were selected from a phage display library consisting of 13 billion clones of protein scaffolds with randomized amino acids in their interaction loops (Supplementary Fig. 1A). The affimer screening over isolated phosvitin was performed by the affimer screening facility of the University of Leeds (Leeds, UK). Briefly, the proteins were biotinylated using EZ-link NHS-SS-biotin (Pierce), then the biotinylated proteins were immobilized on streptavidin-coated wells (Pierce) for 1 h. Phage screening was performed according to the previously described protocol (Tiede et al., 2014) with a minor modification using bovine serum albumin (BSA) as a blocking buffer. 3 % BSA in 1x PBS supplemented with 0.1 % (v/v) TweenTM 20, was used as a blocking buffer. Biopanning resulted in 48 randomly picked positive affimer clones, which were evaluated for their binding affinity to phosvitin by phage ELISA (Supplementary Fig. 1B). The screening led to the selection of three unique phosvitin binders that were further engineered to include cysteine for subsequent labelling. The amino acid composition of their specific variable regions is provided in the Supplementary Fig. 1C. As a control for the binding specificity of the affimers a nonspecific affimer was generated by inserting four alanine amino acids in the first variable loop. The theoretical net charge of the affimers and phosvitin was computed using the amino acid sequence of the proteins and Prot pi calculator (Supplementary Fig. 1D). At pH 6 and 7, both the phosvitin-binding affimers and the control affimers exhibit slightly positive net charges when compared to the highly negatively charged phosvitin. At pH 6, the phosvitin-specific affimers (Pvt-28, Pvt-33, and Pvt-7) have positively charged variable regions. The alanine affimer, lacking charged residues in Loop 1, has a net negative charge due to the glutamic acid (E) in Loop 2. The affimers were labeled via their single cysteine moiety with a maleimide functionalized fluorescent dye for bioimaging.

2.7. Sample preparations and image acquisition

For RCM imaging, 5 µL of BODIPY 493/503 (TCI America, ref. D4341) 1 mg/mL in DMSO was added to 495 µL of the emulsion. After a quick vortex, the emulsion was mixed with 100 µL of phosvitin primary antibody conjugated with Alexa Fluor 647 (sc-46681, Santa Cruz Biotechnology) at a concentration of 20 μg/mL diluted in PBS buffer. For CLSM imaging, 100 µL of phosvitin antibody conjugated with Alexa Fluor 647 (20 $\mu g/mL$ diluted in PBS) was added to 500 μL of the covalently labeled phosvitin-FITC emulsion. For STORM imaging, the phosvitin antibody conjugated with Alexa-647 (sc-46681, Santa Cruz Biotechnology) stock solution was diluted 50 times in PBS buffer. 10 % v/v of the diluted solution was added to 400 μL of the phosvitincontaining model emulsion. After a 15-min incubation at room temperature, all labeled emulsions were centrifuged at 4000 g for 5 min, and the cream layer on top was harvested for imaging. In this cream phase, droplets are prevented from diffusing in the water phase during image acquisition. 2 μL of the cream phase was attentively pipetted into a silicone gasket's well (Grace Bio-Labs). Further, to increase the number of fluorophore blinking events, 25 μL of STORM buffer containing 50 mM TRIS pH 8, 10 mM NaCl, 10 % glucose, 140 mM 2-mercaptoethanol, 68 μg/mL catalase, and 200 μg/mL glucose oxidase was added (Jimenez et al., 2020). A second cover glass was put on the well to prevent new

oxygen from getting into the sample. For each sample we acquired a total of five different field of views.

2.8. Image visualization and data analysis

To analyze the confocal microscope images, we first normalized the contrast of the images from different channels using ImageJ/Fiji (Schindelin et al., 2012). Next, we used StarDist segmentation (Schmidt et al., 2018; Weigert et al., 2020) to extract the positions of individual droplets within the field of view after training the model on multiple datasets using QuPath (Bankhead et al., 2017). For the phosvitin antibody channel (magenta), the image was subtracted from the BODIPY channel (green) to eliminate background interference. We then compared the number of droplets covered with phosvitin to the total number of droplets in the field of view. To assess emulsifier adsorption in relation to droplet size, we computed the Sauter mean diameter, $D_{3,2}$, for all samples within each channel. Specifically, we calculated the diameter of each segmented droplet based on the area obtained with StarDist assuming a perfect circle $(A_i = \pi d_i^2/4)$. Then, we calculated $D_{3,2}$ as $D_{3,2} = \sum d_i^3 / \sum d_i^2$. To specify the width of the droplet size distribution, we took its standard deviation. To analyze the dSTORM raw data, we first removed the constant fluorescence background using a temporal median filter (Jabermoradi et al., 2022) available at GitHub (https://github.com/HohlbeinLab/FTM2). Next, we phasor-based localization algorithm (Martens et al., 2018) implemented in ThunderSTORM (Ovesný et al., 2014), a software plugin for Image-J/Fiji, to determine the positions of the fluorophores with sub-pixel localization precision. For image background filtering in Thunder-STORM, a β -spline wavelet filter with order 2 and scale 3 was used. We applied 2D cross-correlation drift correction with ThunderSTORM settings of $10\times$ bins and $5\times$ magnification. The localizations were then visualized using the "average shifted histogram" option, with the magnification set to 5 and the labeled protein phosvitin represented in magenta. To analyze the distribution of proteins at the interface of individual droplets, we applied droplet segmentation to extract the localizations for each droplet. This allowed us to apply relative position distribution (RPD) analysis (Curd et al., 2021) to quantify the spatial heterogeneity of localizations within droplets, as recently demonstrated (Jabermoradi et al., 2024).

3. Results and discussion

3.1. Localization of covalently and non-covalently labeled phosvitin at droplet interfaces

First, we evaluated the use of affimers to target phosvitin at droplet interfaces. After raising the affimers in a phage display, we selected three candidates Pvt-7, Pvt-28, and Pvt-33 (see also Supplementary Fig. 1). When testing the binding specificity in our phosvitin/SDS model emulsion, only the commercially available antibody against phosvitin showed accumulation at the droplet interface whereas Pvt-28 and a control affimer, in which the targeting residues were replaced by alanine, showed no specificity and were homogenously distributed in the water phase (Supplementary Fig. 2). A similar distribution of affimers was found in emulsions with solely SDS as an anionic emulsifier or Tween20 as a neutral emulsifier, with the latter showing overall reduced fluorescence intensity (Supplementary Fig. 3). Notably, the affimers tend to accumulate around voids, probably representing pockets of air that do not show fluorescence from the lipophilic BODIPY 493/503 that we used to stain the oil droplets (Supplementary Figs. 2-4). Similar to Pvt-28, also Pvt-7 and Pvt-33 did not show any specificity (Supplementary Fig. 4).

Consequently, we chose phosvitin antibodies for our subsequent RCM and STORM investigations of droplet surface coverage. To check the viability of this approach, we first imaged phosvitin covalently labeled with fluorescein isothiocyanate (FITC) in the model emulsion (Fig. 1A). We then imaged the primary phosvitin antibodies conjugated to Alexa Fluor 647 present in the same sample (Fig. 1B). The overlay of the FITC labeled phosvitin and the fluorescently labeled antibody showed good overlap indicating that the antibody successfully targeted the phosvitin (Fig. 1C)

As expected, using the antibody in model emulsions prepared with either SDS or Tween20 but without phosvitin, showed no accumulation at the droplet interfaces (Supplementary Fig. 5). Additionally, we used droplet segmentation to verify that the number of droplets recognized by the antibody matched those stained with FITC (Supplementary Fig. 6). The data further indicate intra-droplet heterogeneity in the coverage of the oil/water interfaces with phosvitin (Fig. 1D).

3.2. Effect of the phosvitin to SDS concentration ratio on the surface coverage of droplets

As phosvitin alone is not an effective emulsifying agent (Castellani et al., 2006; Dickinson et al., 1991), achieving a stable emulsion required the addition of SDS. To obtain insights in the competition and interactions between phosvitin and SDS, we stained the oil droplets with BODIPY 493/503 and kept the concentration of SDS fixed at 1.5 mg/ml (5.2 mM). We then changed the concentration of phosvitin consecutively from 3 mg/mL to 12 mg/mL (0.09–0.34 mM) (Fig. 2). The chosen concentrations for SDS and the lowest considered concentration of phosvitin were selected to ensure full potential coverage of the surface of all oil droplets (Supplementary Material 1). Whereas BODIPY 493/503 (green channel) stains the oil droplets homogeneously (Fig. 2, first column), the fluorescence measured from the phosvitin antibody (magenta channel) is not confined to the interface of the droplets (Fig. 2, second column). In fact, we observe a rather hazy intensity distribution, which we attribute to (1) the presence of phosvitin in the water phase, (2) droplets that are either below or above the imaged volume, and (3) the high number of the droplets in the field of view. Merging both channels revealed that some oil droplets in the green channel are encircled by magenta rings, indicating their coverage by phosvitin (Fig. 2, third column). Importantly, in this system, where only phosvitin and SDS serve as emulsifying agents, droplets that are devoid of phosvitin coverage can be inferred to be coated by SDS. Coverage by SDS is supported by the long-term physical stability of the binary SDS/phosvitin emulsions, which can only be achieved with an emulsifier. Droplets not visibly covered by phosyitin will henceforth be referred to as SDS-covered droplets. We employed the segmentation tool StarDist (Schmidt et al., 2018; Weigert et al., 2020) to segment the droplets in both the green (BODIPY) and magenta (phosvitin) channels. We employed the green channel as a reference to subtract the magenta channel. We achieved a reliable segmentation of the phosvitin-coated droplets (Fig. 2, fourth column) and the droplets in the BODIPY channel (Fig. 2, fifth column). Decreasing concentrations of phosvitin (from top to bottom) are accompanied by decreasing numbers of phosvitin coated droplets in the field of view.

3.3. Quantifying the heterogeneity of droplet coverage at the inter-droplet level

Using the data shown in Fig. 2, we then analyzed the size distribution for droplets predominantly covered by SDS or phosvitin. The histograms show that as the concentration of phosvitin increased, the number of droplets covered by phosvitin increased, whereas the number of SDS droplets declined (Fig. 3). The overall data indicate that phosvitin tends to adsorb at larger droplets. SDS on the other hand, consistently coated smaller droplets across all samples. We computed the surface volume mean diameter (Sauter mean diameter, $D_{3,2}$) for the emulsions depicted in Figs. 2 and 3. This metric quantified the tendencies visually observed in the histogram (Fig. 4A). For all concentrations of phosvitin, we obtained $D_{3,2}$ values between 2.08 and 2.28 \pm 0.7 μ m, and for SDS $D_{3,2}$

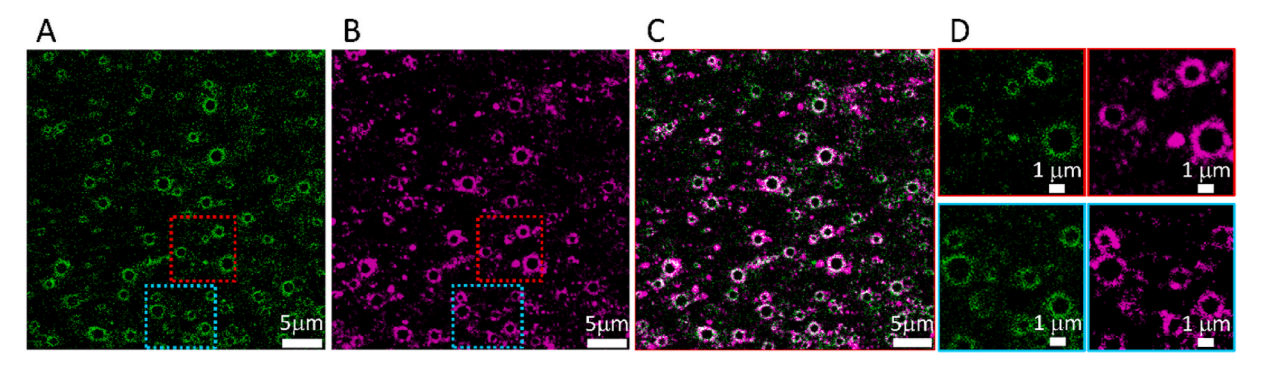


Fig. 1. Dual-color CLSM imaging of a model emulsion stabilized with 0.15 % w/v SDS and FITC-conjugated phosvitin. A) Phosvitin covalently labeled with FITC (green channel), B) Phosvitin antibody covalently labeled with Alexa Fluor 647 (magenta channel), C) Overlay image (green: phosvitin-FITC, magenta: phosvitin antibody, white: co-localization of phosphytin-FITC and phosvitin antibody), and D) The zoomed-in areas of the squared regions in A and B. (For interpretation of the references to color in this figure legend, the reader is referred to the Web version of this article.)

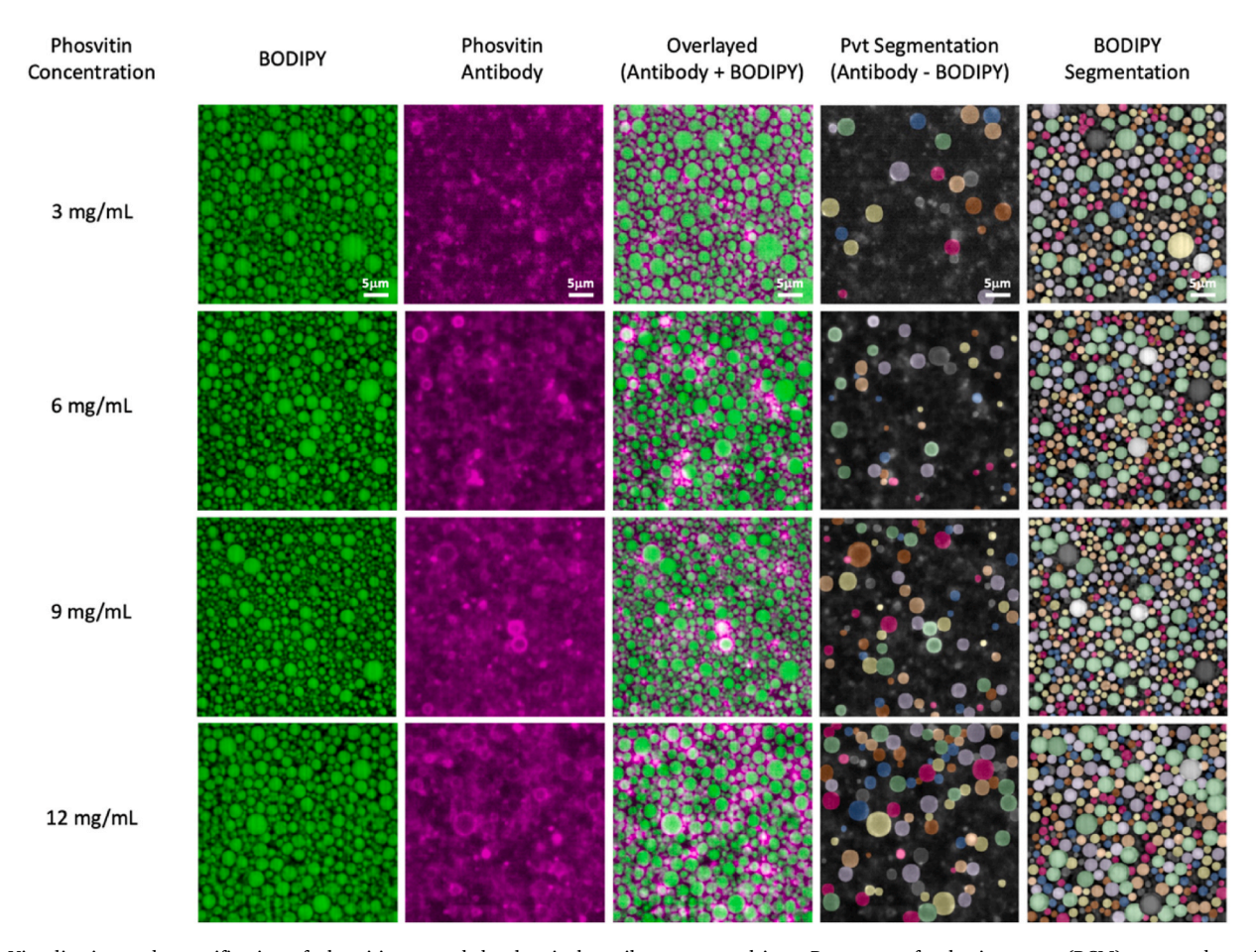


Fig. 2. Visualization and quantification of phosvitin-covered droplets in low-oil-content emulsions. Re-scan confocal microscopy (RCM) was used to visualize phosvitin-coated droplets in emulsions with varying phosvitin concentrations and a constant SDS concentration (1.5 mg/mL). The BODIPY column visualizes all oil droplets labeled by BODIPY 493/503 (represented in the green channel), while the antibody column visualizes phosvitin-coated droplets (shown in the magenta channel) that were identified using Alexa Fluor 647-labeled primary phosvitin antibodies. The merged column shows the overlay of the antibody and BODIPY columns. The Pvt segmentation column demonstrates the result of subtracting the antibody column from the BODIPY column, a step necessary for the segmentation of phosvitin-covered droplets due to the noise present in the antibody channel. The BODIPY segmentation column presents the segmentation of all droplets using the BODIPY column. As demonstrated, the number of identified droplets covered by phosvitin increases with increasing concentrations of phosvitin. (For interpretation of the references to color in this figure legend, the reader is referred to the Web version of this article.)

values between 1.52 and 1.59 \pm 0.5 μ m. The larger $D_{3,2}$ values for phosvitin confirm the protein's tendency to associate with larger droplets, and the $D_{3,2}$ for SDS align with the surfactant's observed preference for smaller droplets. For both phosvitin and SDS droplets, the $D_{3,2}$ values do not vary with concentration, indicating that regardless of the

concentration of the emulsifiers, they adsorb to specific droplet sizes ranges (Fig. 4A).

An explanation of these results lies in the events occurring during the process of high-pressure homogenization (HPH). In our binary model emulsion, both SDS and phosvitin are present in the aqueous phase from

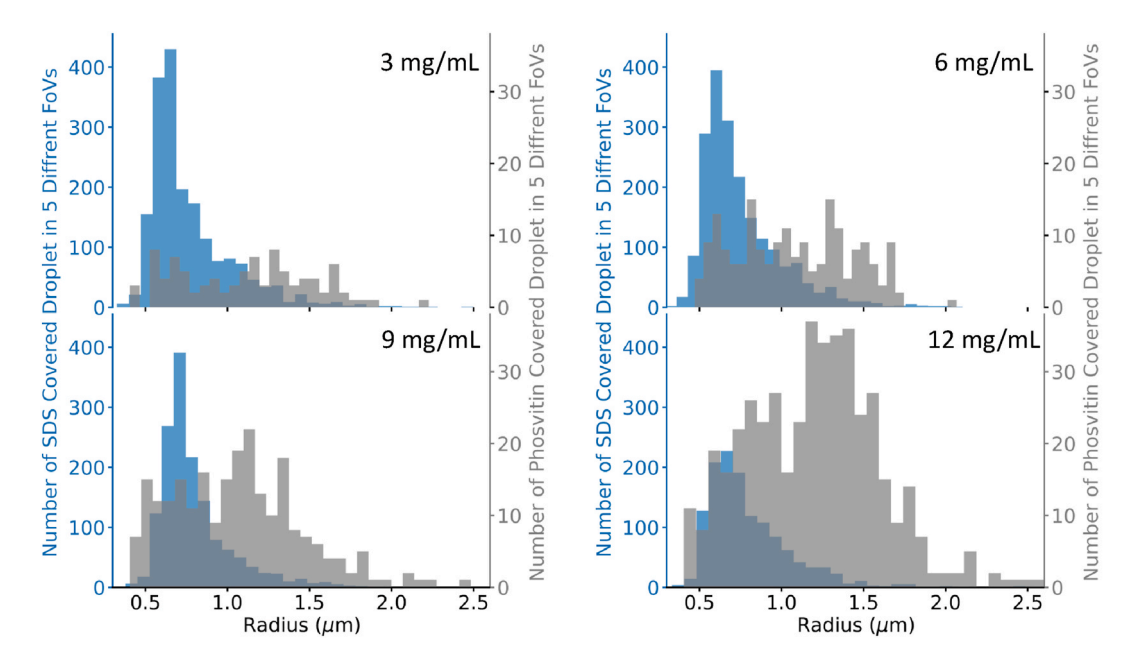


Fig. 3. Assessment of inter-droplet heterogeneity and the impact of various phosvitin concentrations, with a constant SDS concentration (1.5 mg/mL), on droplet size distribution post-segmentation as obtained from RCM images. The histograms display the relative distribution of SDS-covered droplets (blue bars) versus phosvitin-covered droplets (gray bars). Note that phosvitin covered droplets were identified directly in the RCM images, non-covered droplet stained with BODIPY were assumed to be covered with SDS only (see text). For clearer comparisons, droplet counts were adjusted to a reference: maximum observed counts of 450 for SDS droplets in the 3 mg/mL sample and 40 for phosvitin droplets in the 12 mg/mL sample. Increasing the phosvitin concentrations from 3 mg/mL to 12 mg/mL led to a corresponding rise in the proportion of droplets covered by phosvitin, from 10 % (38 out of a total of 400 droplets) to 14 % (54/390), 19 % (71/373), and 25 % (89/358), respectively; The reported droplet counts are based on observations from five different fields of view (FOVs). (For interpretation of the references to color in this figure legend, the reader is referred to the Web version of this article.)

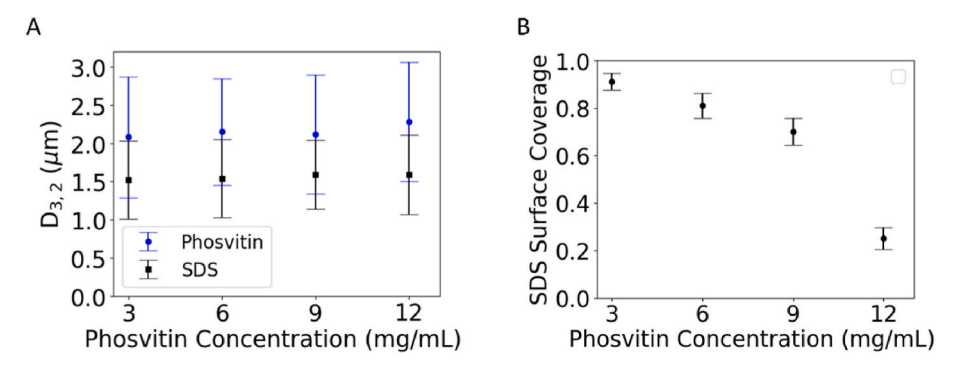


Fig. 4. A) Plot of the surface volume mean diameter $D_{3,2}$ for emulsion samples with varying phosvitin concentrations with a constant SDS concentration (1.5 mg/mL). The circle marker represents the $D_{3,2}$ for phosvitin, the square marker indicates the $D_{3,2}$ for SDS. The larger mean $D_{3,2}$ of phosvitin compared to SDS indicates a tendency of phosvitin to associate with larger droplets. B) Plot illustrating the SDS area coverage across various phosvitin concentrations with a constant SDS concentration (1.5 mg/mL).

the onset of the coarse homogenization step using a high-shear mixer. The coarse droplets are likely stabilized by a mix of SDS and phosvitin. Subsequently, HPH fragments the pre-homogenized, coarse droplets into smaller ones. This fragmentation leads to a rapid increase of the total surface area, which needs to be stabilized by emulsifiers. Immediately after their formation, the fine droplets have virtually bare interfaces prone to coalescence until their surfaces have accumulated a sufficient coverage of SDS and/or phosvitin. Moreover, the coalescence itself will contribute to the increase of interfacial coverage because the coarsening implies a reduction in interfacial area. Since the adsorption kinetics of the small molecule SDS is faster than that of the macromolecule phosvitin, the small(est) droplets in the size distribution will get stabilized by SDS before much phosvitin has adsorbed.

On the other hand, larger droplets coalesce more slowly, thereby providing sufficient time for proteins to adsorb. As these droplets coalesce, their mixed interfaces of phosvitin and SDS become denser.

However, while protein adsorption is quasi-irreversible (Jafari et al., 2008), SDS dynamically exchanges with the bulk, leading to the detachment of surplus SDS as the protein concentration increases. This process yields larger droplets that are primarily covered by proteins. Consequentially, in oil/water emulsions with SDS and phosvitin, phosvitin plays a more dominant role in the stabilization of larger droplets.

The competition between SDS and phosvitin is shown in Fig. 4B, which depicts the SDS area coverage against the concentrations of phosvitin. At the lowest concentration of phosvitin, 91 % of the surface area is covered by SDS. However, as the concentration of phosvitin increases, the proportion of droplet surface area covered by SDS consistently decreases. It is important to note that both SDS and phosvitin were present at sufficiently high concentrations to cover all droplets (Supplementary Material 1). The observed decrease in SDS droplet surface coverage with increasing phosvitin concentration indicates an inherent competition between these emulsifiers for covering droplet

interfaces within the binary emulsion.

3.4. Quantifying the heterogeneity of droplet coverage at the intra-droplet level

Next, we proceeded with STORM to further quantify the intradroplet distribution of phosvitin. The STORM images in Fig. 5A show that an increase in the concentration of phosvitin results in an increased number of large droplets covered. This experiment validates the findings from the RCM experiments showing an increase in the percentage of droplets covered by phosvitin with increasing concentration of phosvitin. The enhanced spatial resolution of STORM allowed assessment of the intra-droplet surface heterogeneity of droplets that were at least partially covered with phosvitin. We quantified the spatial heterogeneity of phosvitin localizations at the surface of single droplets with a methodology described previously that uses all localizations in individual droplets to calculate relative position distances (RPD) (Jabermoradi et al., 2024). This approach leads histograms that provide a fingerprint of intra-droplet heterogeneity of interfacial coverage (Fig. 5B). Qualitatively, there was no significant influence of phosvitin concentration on the shape of the histograms. Further, we calculated RPD histograms for droplet sizes below and above the average $D_{3,2}$ value which also appeared similar (Supplementary Fig. 7). We used the chi-squared test for assessment of significant differences between the RPDs shown in Fig. 5 since we deemed it suitable for categorical distributions (Supplementary Table 2). This test did not reveal significant differences. For a more quantitative assessment, we calculated the relative peak amplitudes $A_{\rm rel}$ - a metric representing the ratio of the first peak's amplitude to the sum of the first and second peaks, for the two droplet size populations for each concentration. All relative peak amplitudes were approximately 0.39, indicating a partially heterogeneous distribution of phosvitin (Supplementary Fig. 7). We conclude that neither the droplet size nor the concentration of phosvitin affected the perceived heterogeneity of the distribution of phosvitin on the droplet interfaces of our model emulsions after HPH. The latter finding can be explained by the coalescence of smaller droplets formed during HPH. During coalescence, SDS is partially expelled from the interface thereby leading to an increasing concentration of phosvitin. As such the original SDS/phosvitin ratio can lead to similar heterogeneous distributions of phosvitin at the interface.

3.5. Impact of low shear treatment on the surface coverage with phosvitin

Finally, we investigated the impact of low-shear treatment, which allows for diffusion-assisted exchange of SDS and phosvitin between droplet interfaces and with the continuous aqueous phase. For this purpose, we selected the binary SDS/phosvitin emulsion with a phosvitin concentration of 6 mg/mL. Following the initial HPH, the emulsion was subjected to low shear using a roller shaker for a duration of 3 days. To assess the influence of this processing step on the emulsion, we employed STORM before and after low-shear treatment (Fig. 6A).

After the low shear treatment, we saw a reduction in the number of phosvitin-covered droplets (Fig. 6B). The redistribution of SDS over the droplet surface is visualized in the histograms in Fig. 6C and D. Post lowshear treatment, the histogram (Fig. 6D) shows that the distribution of SDS-covered droplets remained constant. However, the number of phosvitin-covered droplets diminished, indicating that phosvitin was displaced by SDS from the droplet interfaces. To verify whether droplet coalescence played a role, we calculated the $D_{3,2}$, which remained constant at approximately 1.73 \pm 0.56 μm and 1.72 \pm 0.61 μm before and after low-shear treatment, respectively. Thus, droplet coalescence can be excluded to play a role during low shear treatment. We therefore attribute the replacement of phosvitin by SDS to a slow equilibration towards a more thermodynamically favorable state in which droplet interfaces are solely covered by SDS. To ensure that the observed decrease in phosvitin coverage was not due to aging of the emulsion, we also measured a control sample from the same stock kept at room temperature that had not been sheared for three days. Upon imaging the control sample, we observed results consistent with Fig. 6A, indicating that ageing without shear treatment did not cause a decrease in phosvitin coverage (Supplementary Fig. 8).

We then quantified the intra-droplet phosvitin distribution at the interface for all droplets within the field of view post low-shear treatment (Fig. 6E). The relative peak amplitude, $A_{\rm rel}$ for droplet with sizes below and above $D_{3,2}$ were respectively 0.47 \pm 0.19 and 0.49 \pm 0.18. These values are not different from each other, and not significantly different from the $A_{\rm rel}$ obtained before the low-shear treatment, with values of 0.4 \pm 0.14 and 0.35 \pm 0.15 for droplet sizes below and above

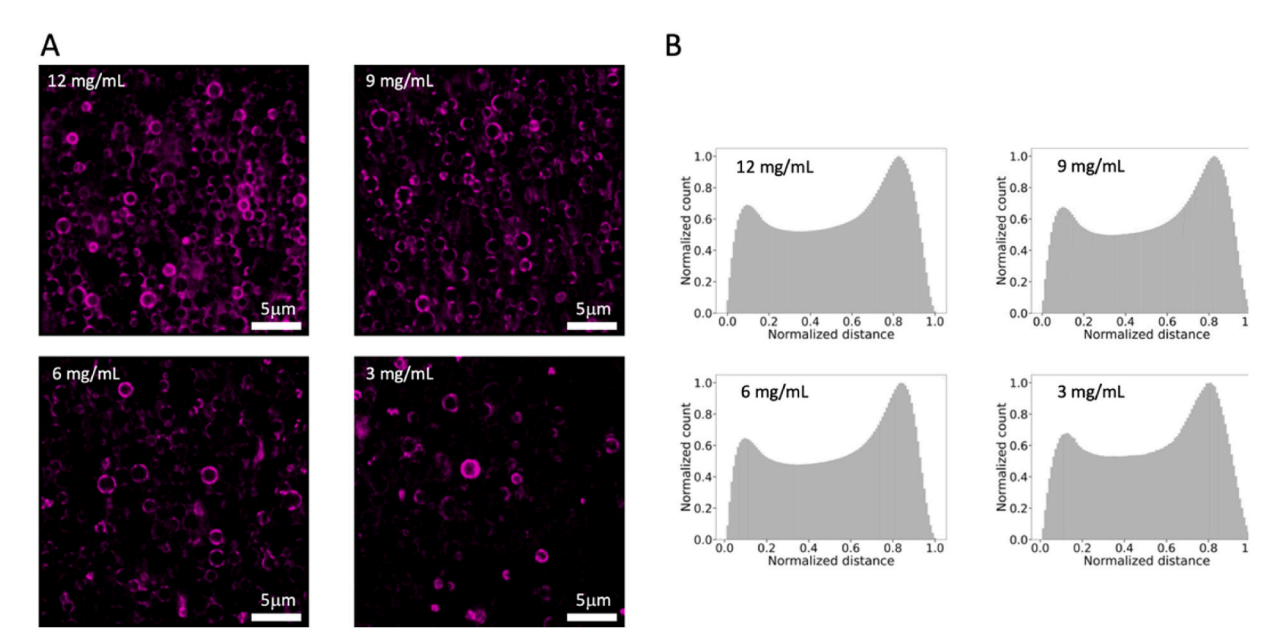


Fig. 5. Analysing the intra-droplet heterogeneity of the distribution of phosvitin at droplet interfaces. A) STORM microscopy images of phosvitin at droplet interfaces at different concentrations. B) Histograms of normalized relative position distances (RPD) were used to analyze the intra-droplet heterogeneity of the phosvitin distribution. RPD distances were normalized and averaged across all droplets for each concentration.

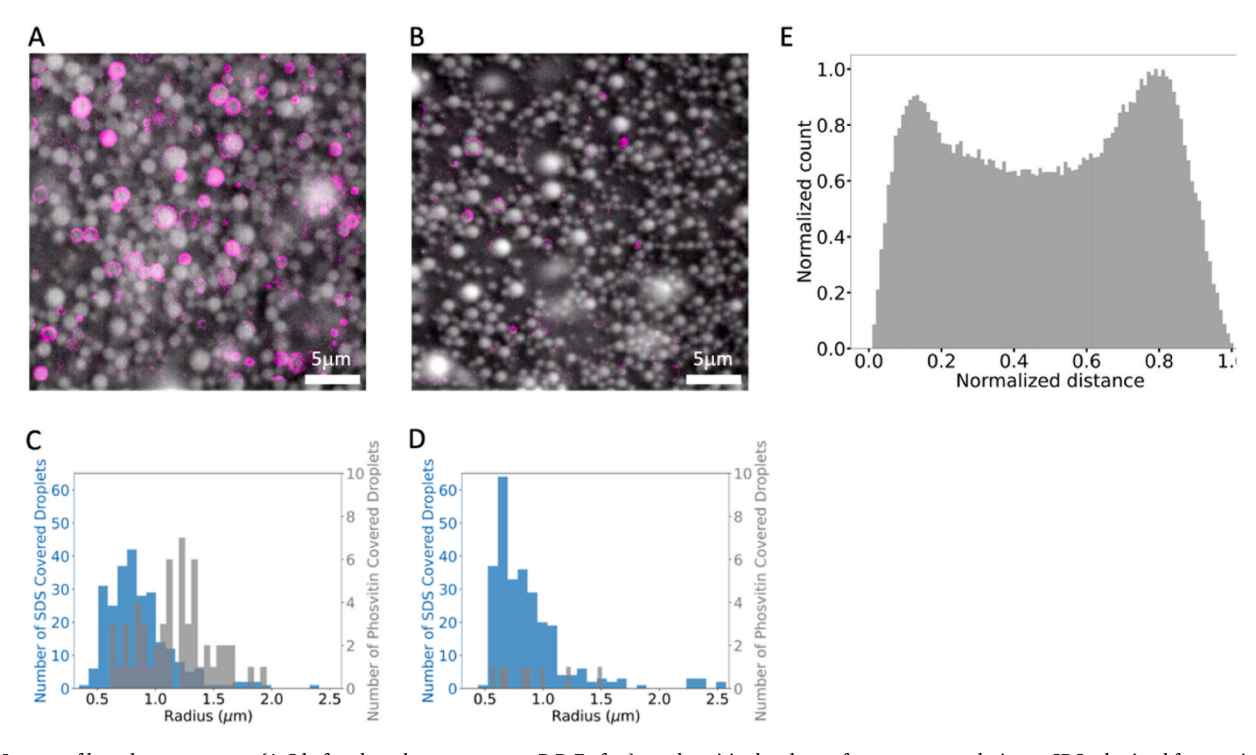


Fig. 6. Impact of low shear treatment (A,C before low shear treatment; B,D,E after) on phosvitin droplet surface coverage relative to SDS, obtained from a single field of view (FOV). Note that phosvitin covered droplets can be identified directly in STORM images, non-covered droplets are assumed to be covered with SDS (see text). A) Merge of the STORM image (magenta channel) and the bright field of the emulsion sample before low shear treatment. The total number of droplets covered by SDS is 256. B) Same as in A with a total of 273 droplets covered by SDS, but after low shear treatment. The histograms display the relative distribution of SDS-covered droplets (blue bars) versus phosvitin-covered droplets (gray bars) C) Before low shear treat ment, and D) After low shear treatment. E) Histograms of the normalized RPD to examine the heterogeneity of phosvitin distribution post low-shear treatment. RPD distances were normalized and averaged across all droplets within the field of view. (For interpretation of the references to color in this figure legend, the reader is referred to the Web version of this article.)

 $D_{3,2}$, respectively. Our results are in line with previous findings that in O/W emulsions the droplet coverage with low molecular weight surfactants is thermodynamically favored over coverage with proteins. This effect can be understood by the stronger ability of low molecular weight surfactants to lower surface tension (Nylander et al., 2019; Pugnaloni et al., 2004).

This effect was also observed for full mayonnaise subjected to a prolonged low shear treatment (Serial et al., 2022). These previous findings were, however, mostly underpinned with indirect measurements of droplet surfactant coverage, whereas our super-resolution approach provides direct visualization with inter- and intra-droplet resolution.

3.6. From simplified model systems to investigating more complex food systems

Whereas we here focused on a simplified SDS/phosvitin model system, the general methodology is applicable to more complex food systems. In our recent work on whey protein isolate-stabilized emulsions, we employed diffraction-limited fluorescence microscopy revealing heterogeneity of oxidized proteins covering micrometer sized oil droplets (Yang et al., 2024). The fluorophore used there to target oxidized protein residues, CAMPO-AF647 is in principle compatible with the STORM approaches used here thereby allowing to super-resolve protein localizations at interfaces and to apply the quantitative RPD framework (Jabermoradi et al., 2024). We note, that with increasing oil content or overall increasing surface area, there are practical limitations in using specifically made fluorophores or antibodies. First, a higher oil content will lead to optical aberrations that increase in strength the further away from the cover slide the sample is illuminated. Here, adaptive optics in combination with SMLM microscopy is an option to minimize the effect of aberrations (Jabermoradi et al., 2022). Second, premixing of reagents

before preparing the emulsion could be costly, depending on the minimal volume by which the emulsion can be prepared effectively. Third, albeit we here successfully employed antibodies against phosvitin, the relatively large size of antibodies (5–10 nm) will limit the obtainable localization accuracy and thereby the quantitative assessment of phosvitin copy numbers. Along the same lines, the availability of efficient antibodies against proteins of interest is crucial. In some preliminary experiments, we have successfully tested the primary human apoB mouse antibody targeting apoproteins in egg yolk in combination with fluorescently labeled, secondary mouse antibodies (data not shown). Ultimately, we believe that the spatially and temporally resolved mapping of emulsifiers can guide the formulation of emulsions by offering clear readouts of properties that are otherwise difficult to assess.

4. Conclusion

Phosvitin-binding affimers that were specifically raised against phosvitin in a phage display, did not show sufficient specificity at the at the oil-water interface of HPH manufactured SDS/phosvitin model emulsions. In contrast, phosvitin-binding antibodies showed the required high specificity for localization at droplet interfaces. Re-scan confocal microscopy revealed that for HPH manufactured O/W model emulsions a bimodal droplet size was obtained wherein small droplets were solely covered by SDS and large droplets predominantly by phosvitin. This inter-droplet heterogeneity in the coverage of droplets was in line with the time-evolution of the emulsifier coverage of droplet interfaces during HPH. STORM indicated that the concentration of phosvitin did not affect the intra-droplet distribution at the droplet interface. STORM also provided a direct visualization of the redistribution of phosvitin upon low shear treatment, which hitherto could only be inferred from indirect measurements. Our RCM- and STORM-based approaches allow a direct and quantitative view on the intricate balance

between kinetic and thermodynamic forces governing the intra- and inter-droplet interfacial distribution of proteins, paving the way for new studies in the realm of research on food emulsions.

CRediT authorship contribution statement

Abbas Jabermoradi: Writing – review & editing, Writing – original draft, Visualization, Validation, Software, Methodology, Investigation, Formal analysis, Data curation. Sanam Foroutanparsa: Writing – review & editing, Visualization, Validation, Methodology, Investigation, Formal analysis. Ilja K. Voets: Writing – review & editing, Validation, Supervision, Methodology, Funding acquisition, Conceptualization. Jo J.M. Janssen: Validation. John P.M. van Duynhoven: Writing – review & editing, Validation, Supervision, Methodology, Funding acquisition, Conceptualization. Johannes Hohlbein: Writing – review & editing, Validation, Supervision, Methodology, Funding acquisition, Conceptualization.

Data availability

Data (*.tiff and *.csv files of raw data or analyzed raw image data) have been deposited here: https://doi.org/10.5281/zenodo.14801229

Funding

This publication is part of the project Localbiofood (with project number 731.017.204) of the research program Science PPP Fund, which is (partly) financed by the Dutch Research Council (NWO) in collaboration with ChemistryNL. This work is further part of the research program LICENSE with project number 731.017.301, which is financed by the Dutch Research Council (NWO).

Declaration of competing interest

The authors declare the following financial interests/personal relationships which may be considered as potential competing interests: J. J.M.J. and J.P.M.v.D. are employed by a company that manufactures and markets mayonnaise. The other authors declare that they have no known competing financial interests or personal relationships that could influence the work reported in this paper.

Acknowledgments

We would like to thank our colleagues in both consortia (Local-BioFood and LICENSE) and the Laboratory of Biophysics for helpful discussions. We kindly acknowledge the Dr. C. Tiede, Prof. D. Tomlinson, and Prof. M. McPherson from the University of Leeds for raising the affimers and for helpful discussions on their properties and application.

Appendix A. Supplementary data

Supplementary data to this article can be found online at https://doi.org/10.1016/j.foodhyd.2025.111490.

Data availability

Manuscript contains link to a data repository (Zenodo)

References

- Anton, M. (2013). Egg yolk: Structures, functionalities and processes: Egg yolk: Structures, functionalities and processes. *Journal of the Science of Food and Agriculture*, 93(12), 2871–2880. https://doi.org/10.1002/isfa.6247
- Bankhead, P., Loughrey, M. B., Fernández, J. A., Dombrowski, Y., McArt, D. G., Dunne, P. D., ... Hamilton, P. W. (2017). QuPath: Open source software for digital pathology image analysis. *Scientific Reports*, 7(1), 16878. https://doi.org/10.1038/ s41598-017-17204-5

- Banta, S., Dooley, K., & Shur, O. (2013). Replacing antibodies: Engineering new binding proteins. Annual Review of Biomedical Engineering, 15(1), 93–113. https://doi.org/ 10.1146/annurev-bioeng-071812-152412
- Berton-Carabin, C., & Villeneuve, P. (2023). Targeting interfacial location of phenolic antioxidants in emulsions: Strategies and benefits. *Annual Review of Food Science and Technology*, 14(1), 63–83. https://doi.org/10.1146/annurev-food-060721-021636
- Bradbury, A., & Plückthun, A. (2015). Reproducibility: Standardize antibodies used in research. *Nature*, 518(7537), 27–29. https://doi.org/10.1038/518027a
- Castellani, O., Belhomme, C., David-Briand, E., Guérin-Dubiard, C., & Anton, M. (2006). Oil-in-water emulsion properties and interfacial characteristics of hen egg yolk phosvitin. Food Hydrocolloids, 20(1), 35–43. https://doi.org/10.1016/j. foodhyd.2005.02.010
- Castellani, O., Martinet, V., David-Briand, E., Guérin-Dubiard, C., & Anton, M. (2003).
 Egg yolk phosvitin: Preparation of metal-free purified protein by fast protein liquid chromatography using aqueous solvents. *Journal of Chromatography B*, 791(1–2), 273–284. https://doi.org/10.1016/51570-0232(03)00230-7
- Cornec, M., Wilde, P. J., Gunning, P. A., Mackie, A. R., Husband, F. A., Parker, M. L., & Clark, D. C. (1998). Emulsion stability as affected by competitive adsorption between an oil-soluble emulsifier and milk proteins at the interface. *Journal of Food Science*, 63(1), 39–43. https://doi.org/10.1111/j.1365-2621.1998.tb15671.x
- Curd, A. P., Leng, J., Hughes, R. E., Cleasby, A. J., Rogers, B., Trinh, C. H., Baird, M. A., Takagi, Y., Tiede, C., Sieben, C., Manley, S., Schlichthaerle, T., Jungmann, R., Ries, J., Shroff, H., & Peckham, M. (2021). Nanoscale pattern extraction from relative positions of sparse 3D localizations. *Nano Letters*, 21(3), 1213–1220. https://doi.org/10.1021/acs.nanolett.0c03332
- De Luca, G. M. R., Breedijk, R. M. P., Brandt, R. A. J., Zeelenberg, C. H. C., de Jong, B. E., Timmermans, W., Azar, L. N., Hoebe, R. A., Stallinga, S., & Manders, E. M. M. (2013). Re-scan confocal microscopy: Scanning twice for better resolution. *Biomedical Optics Express*, 4(11), 2644. https://doi.org/10.1364/BOE.4.002644
- Dickinson, E., Hunt, J. A., & Dalgleish, D. G. (1991). Competitive adsorption of phosvitin with milk proteins in oil-in-water emulsions. *Food Hydrocolloids*, 4(5), 403–414. https://doi.org/10.1016/S0268-005X(09)80135-5
- Ewers, W., & Sutherland, K. (1952). The role of surface transport in the stability and breakdown of foams. Australian Journal of Chemistry, 5(4), 697. https://doi.org/ 10.1071/CH9520697
- Hasenhuettl, G. L., & Hartel, R. W. (Eds.). (2019). Food emulsifiers and their applications. Springer International Publishing. https://doi.org/10.1007/978-3-030-29187-7.
- Hinderink, E. B. A., Meinders, M. B. J., Miller, R., Sagis, L., Schroën, K., & Berton-Carabin, C. C. (2022). Interfacial protein-protein displacement at fluid interfaces. Advances in Colloid and Interface Science, 305, Article 102691. https://doi.org/10.1016/j.cis.2022.102691
- Hinderink, E. B. A., Schroën, K., Sagis, L. M. C., & Berton-Carabin, C. C. (2024). Surface load and interfacial composition of protein-stabilized O/W emulsions. In C. Lopez, C. Genot, & A. Riaublanc (Eds.), Multidimensional characterization of dietary lipids (pp. 317–323). Springer US. https://doi.org/10.1007/978-1-0716-3758-6-22.
- Hohlbein, J. (2021). Single-molecule localization microscopy as an emerging tool to probe multiscale food structures. Food Structure, 30, Article 100236. https://doi.org/ 10.1016/j.foostr.2021.100236
- Jabermoradi, A., van Duynhoven, J. P. M., & Hohlbein, J. (2024). Quantifying the distribution of proteins at the interface of oil-in-water food emulsions. Food Structure, 42, Article 100393. https://doi.org/10.1016/j.foostr.2024.100393
- Jabermoradi, A., Yang, S., Gobes, M. I., van Duynhoven, J. P. M., & Hohlbein, J. (2022). Enabling single-molecule localization microscopy in turbid food emulsions. Philosophical Transactions of the Royal Society A: Mathematical, Physical & Engineering Sciences, 380(2220), Article 20200164. https://doi.org/10.1098/rsta.2020.0164
- Jafari, S. M., Assadpoor, E., He, Y., & Bhandari, B. (2008). Re-coalescence of emulsion droplets during high-energy emulsification. Food Hydrocolloids, 22(7), 1191–1202. https://doi.org/10.1016/j.foodhyd.2007.09.006
- Javadi, A., Dowlati, S., Shourni, S., Miller, R., Kraume, M., Kopka, K., & Eckert, K. (2022). Experimental techniques to study protein–surfactant interactions: New insights into competitive adsorptions via drop subphase and interface exchange. Advances in Colloid and Interface Science, 301, Article 102601. https://doi.org/10.1016/j.cis.2022.102601
- Jimenez, A., Friedl, K., & Leterrier, C. (2020). About samples, giving examples: Optimized single molecule localization microscopy. *Methods*, 174, 100–114. https://doi.org/10.1016/j.ymeth.2019.05.008
- Kokini, J., & Aken, G. van (2006). Discussion session on food emulsions and foams. Food Hydrocolloids, 20(4), 438–445. https://doi.org/10.1016/j.foodhyd.2005.10.003
- Maldonado-Valderrama, J., & Patino, J. M. R. (2010). Interfacial rheology of protein–surfactant mixtures. Current Opinion in Colloid & Interface Science, 15(4), 271–282. https://doi.org/10.1016/j.cocis.2009.12.004
- Marcet, I., Sáez-Orviz, S., Rendueles, M., & Díaz, M. (2022). Egg yolk granules and phosvitin. Recent advances in food technology and applications. *LWT*, 153, Article 112442. https://doi.org/10.1016/j.lwt.2021.112442
- Martens, K. J. A., Bader, A. N., Baas, S., Rieger, B., & Hohlbein, J. (2018). Phasor based single-molecule localization microscopy in 3D (pSMLM-3D): An algorithm for MHz localization rates using standard CPUs. *The Journal of Chemical Physics*, 148(12), Article 123311. https://doi.org/10.1063/1.5005899
- McClements, D. J. (2015). Food emulsions: Principles, practices, and techniques (3rd ed. (0 ed.)). CRC Press. https://doi.org/10.1201/b18868
- McClements, D. J., & Jafari, S. M. (2018). Improving emulsion formation, stability and performance using mixed emulsifiers: A review. Advances in Colloid and Interface Science, 251, 55–79. https://doi.org/10.1016/j.cis.2017.12.001
- Niu, H., Wang, W., Dou, Z., Chen, X., Chen, X., Chen, H., & Fu, X. (2023). Multiscale combined techniques for evaluating emulsion stability: A critical review. *Advances in*

- Colloid and Interface Science, 311, Article 102813. https://doi.org/10.1016/j.
- Nylander, T., Arnebrant, T., Cárdenas, M., Bos, M., & Wilde, P. (2019). Protein/ emulsifier interactions. In G. L. Hasenhuettl, & R. W. Hartel (Eds.), Food emulsifiers and their applications (pp. 101–192). Springer International Publishing. https://doi. org/10.1007/978-3-030-29187-7_5.
- Orlova, A., Magnusson, M., Eriksson, T. L. J., Nilsson, M., Larsson, B., Höidén-Guthenberg, I., Widström, C., Carlsson, J., Tolmachev, V., Ståhl, S., & Nilsson, F. Y. (2006). Tumor imaging using a picomolar affinity HER2 binding affibody molecule. Cancer Research, 66(8), 4339–4348. https://doi.org/10.1158/0008-5472.CAN-05-3521
- Ovesný, M., Křížek, P., Borkovec, J., Švindrych, Z., & Hagen, G. M. (2014). ThunderSTORM: A comprehensive ImageJ plug-in for palm and STORM data analysis and super-resolution imaging. *Bioinformatics*, 30(16), 2389–2390. https://doi.org/10.1093/bioinformatics/btu202
- Pugnaloni, L. A., Dickinson, E., Ettelaie, R., Mackie, A. R., & Wilde, P. J. (2004). Competitive adsorption of proteins and low-molecular-weight surfactants: Computer simulation and microscopic imaging. Advances in Colloid and Interface Science, 107 (1), 27–49. https://doi.org/10.1016/j.cis.2003.08.003
- Rampon, V., Genot, C., Riaublanc, A., Anton, M., Axelos, M. A. V., & McClements, D. J. (2003). Front-face fluorescence spectroscopy study of globular proteins in emulsions: Displacement of BSA by a nonionic surfactant. *Journal of Agricultural and Food Chemistry*, 51(9), 2482–2489. https://doi.org/10.1021/jf026168g
- Ravera, F., Dziza, K., Santini, E., Cristofolini, L., & Liggieri, L. (2021). Emulsification and emulsion stability: The role of the interfacial properties. Advances in Colloid and Interface Science, 288, Article 102344. https://doi.org/10.1016/j.cis.2020.102344
- Rodríguez Patino, J. M., & Pilosof, A. M. R. (2011). Protein–polysaccharide interactions at fluid interfaces. Food Hydrocolloids, 25(8), 1925–1937. https://doi.org/10.1016/j. foodhyd.2011.02.023
- Rust, M. J., Bates, M., & Zhuang, X. (2006). Sub-diffraction-limit imaging by stochastic optical reconstruction microscopy (STORM). *Nature Methods*, 3(10), 793–796. https://doi.org/10.1038/nmeth929
- Schindelin, J., Arganda-Carreras, I., Frise, E., Kaynig, V., Longair, M., Pietzsch, T., Preibisch, S., Rueden, C., Saalfeld, S., Schmid, B., Tinevez, J.-Y., White, D. J., Hartenstein, V., Eliceiri, K., Tomancak, P., & Cardona, A. (2012). Fiji: An open-source platform for biological-image analysis. *Nature Methods*, 9(7), 676–682. https://doi.org/10.1038/nmeth.2019
- Schlichthaerle, T., Eklund, A. S., Schueder, F., Strauss, M. T., Tiede, C., Curd, A., Ries, J., Peckham, M., Tomlinson, D. C., & Jungmann, R. (2018). Site-specific labeling of affimers for DNA-PAINT microscopy. *Angewandte Chemie International Edition*, 57 (34), 11060–11063. https://doi.org/10.1002/anie.201804020
- Schmidt, U., Weigert, M., Broaddus, C., & Myers, G. (2018). Cell detection with star-convex polygons. In A. F. Frangi, J. A. Schnabel, C. Davatzikos, C. Alberola-López, & G. Fichtinger (Eds.), Medical image computing and computer assisted intervention miccai 2018 (Vol. 11071, pp. 265–273). Springer International Publishing. https://doi.org/10.1007/978-3-030-00934-2 30.

- Serial, M. R., Arnaudov, L. N., Stoyanov, S., Dijksman, J. A., Terenzi, C., & van Duynhoven, J. P. M. (2022). Non-invasive rheo-MRI study of egg yolk-stabilized emulsions: Yield stress decay and protein release. *Molecules*, 27(10), 3070. https://doi.org/10.3390/molecules27103070
- Stuurman, N., Amdodaj, N., & Vale, R. (2007).

 µManager: Open source software for light microscope imaging.

 Microscopy Today, 15(3), 42–43.

 https://doi.org/10.1017/ \$1551929500055541
- Taisne, L., Walstra, P., & Cabane, B. (1996). Transfer of oil between emulsion droplets. Journal of Colloid and Interface Science, 184(2), 378–390. https://doi.org/10.1006/jcis.1996.0632
- Tans, R., van Rijswijck, D. M. H., Davidson, A., Hannam, R., Ricketts, B., Tack, C. J., Wessels, H. J. C. T., Gloerich, J., & van Gool, A. J. (2020). Affimers as an alternative to antibodies for protein biomarker enrichment. *Protein Expression and Purification*, 174, Article 105677. https://doi.org/10.1016/j.pep.2020.105677
- Tiede, C., Bedford, R., Heseltine, S. J., Smith, G., Wijetunga, I., Ross, R., AlQallaf, D., Roberts, A. P., Balls, A., Curd, A., Hughes, R. E., Martin, H., Needham, S. R., Zanetti-Domingues, L. C., Sadigh, Y., Peacock, T. P., Tang, A. A., Gibson, N., Kyle, H., ... Tomlinson, D. C. (2017). Affimer proteins are versatile and renewable affinity reagents. Elife, 6, Article e24903. https://doi.org/10.7554/eLife.24903
- Tiede, C., Tang, A. A. S., Deacon, S. E., Mandal, U., Nettleship, J. E., Owen, R. L., George, S. E., Harrison, D. J., Owens, R. J., Tomlinson, D. C., & McPherson, M. J. (2014). Adhiron: A stable and versatile peptide display scaffold for molecular recognition applications. *Protein Engineering Design and Selection*, 27(5), 145–155. https://doi.org/10.1093/protein/gzu007
- van Aken, G. A. (2003). Competitive adsorption of protein and surfactants in highly concentrated emulsions: Effect on coalescence mechanisms. *Colloids and Surfaces A: Physicochemical and Engineering Aspects*, 213(2–3), 209–219. https://doi.org/ 10.1016/S0927-7757(02)00514-9
- Voskuil, J. (2014). Commercial antibodies and their validation. F1000Research, 3, 232. https://doi.org/10.12688/f1000research.4966.2
- Weigert, M., Schmidt, U., Haase, R., Sugawara, K., & Myers, G. (2020). Star-convex polyhedra for 3D object detection and segmentation in microscopy. 2020 IEEE winter conference on applications of computer vision (WACV). https://doi.org/10.1109/ WACV45572.2020.9093435
- Wilde, P., Mackie, A., Husband, F., Gunning, P., & Morris, V. (2004). Proteins and emulsifiers at liquid interfaces. Advances in Colloid and Interface Science, 108–109, 63–71. https://doi.org/10.1016/j.cis.2003.10.011
- Yang, S., ten Klooster, S., Nguyen, K. A., Hennebelle, M., Berton-Carabin, C. C., Schroën, K., van Duynhoven, J. P. M., & Hohlbein, J. (2024). Droplet size dependency and spatial heterogeneity of lipid oxidation in whey protein isolatestabilized emulsions. Food Research International, 188, Article 114341. https://doi. org/10.1016/j.foodres.2024.114341
- Zhang, X., Qiu, N., Geng, F., & Ma, M. (2011). Simply and effectively preparing high-purity phosvitin using polyethylene glycol and anion-exchange chromatography. *Journal of Separation Science*, 34(22), 3295–3301. https://doi.org/10.1002/issc.201100601